Shorting at Long Duration: Impact of Extended Discharge Capacity on Battery Solid Electrolytes

Ryan C. Hill[a]†, Amanda S. Peretti[b], Leo J. Small[b], Erik D. Spoerke[b], and Yang-Tse Cheng[a]*

a. Department of Chemical and Materials Engineering, University of Kentucky, Lexington, KY 40506, USA.

b. Sandia National Laboratories, Albuquerque, NM 87123, USA

AUTHOR INFORMATION

Corresponding Author

Ryan C. Hill

Department of Chemical and Materials Engineering

University of Kentucky College of Engineering

177 F Paul Anderson Tower

512 Administration Drive

Lexington, KY 40506

Ryan.C.Hill@stonybrook.edu

Abstract

Long-duration energy storage (LDES) is critical to a stable, resilient, and decarbonized electric grid. While batteries are emerging as important LDES devices, extended, high-power discharges necessary for cost-competitive LDES present new materials challenges. Focusing on a new generation of low-temperature molten sodium batteries, we explore here unique phenomena related to long-duration discharge through a well-known solid electrolyte, NaSICON. Specifically, molten sodium symmetric cells at 110 °C were cycled at 0.1 A cm^{-2} for 1-23 h discharges. Longer discharges led to unstable overpotentials, reduced resistances, and decreased electrolyte strength, caused by massive sodium penetration not observed in shorter duration discharges. SEM observations informed mechanisms of sodium penetration and even "healing" during shorter-duration cycling. Importantly, these findings show that traditional, low-capacity, shorter-duration tests may not sufficiently inform fundamental materials phenomena that will impact LDES battery performance. This case highlights the importance that candidate LDES batteries be tested under pertinent long-duration conditions.

TOC GRAPHICS

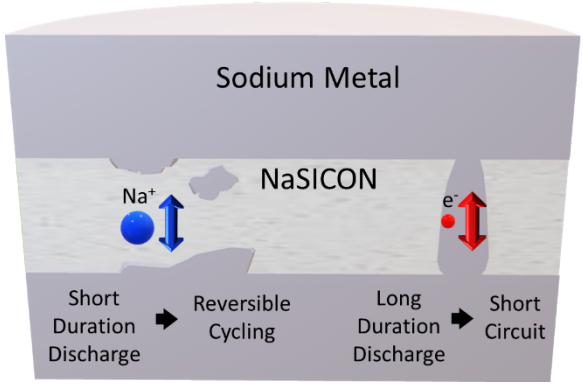

Replacing fossil fuel plants with renewable generators is key to a cleaner, sustainable, and decarbonized electrical grid of the future.[1-5] However, many renewable energy generators rely on energy storage to manage excess generation and inherent renewable intermittency while providing rapid load response flexibility during peak demand periods.[6-11] In addition to this short-term (e.g., 2-4 hour) storage, there is an increasing need to access stored energy in times of extended, unplanned generation outages. For these applications, short-duration storage will not be sufficient to meet demands of the near future; long-duration energy storage (LDES) capable of storage for >10-12 hours, multiday storage, or even seasonal storage will be needed.[12-15] Emerging batteries targeting longer-duration applications show promise for grid integration, owing to their application flexibility and promise of agile, resilient, and long lifetime performance.[16]

Many "beyond Li-ion" chemistries have been explored for LDES due to cost, supply chain, and safety issues associated with Li-ion batteries.[17-20] Molten sodium (Na) batteries, commonly Na-S or ZEBRA chemistries, have particularly piqued interest due to Na's high capacity (1166 mAh g^{-1}), low reduction potential (-2.71 V vs. SHE), and earth abundance.[21, 22] These batteries typically operate above 250 °C and require solid electrolytes, usually β''-alumina (BASE) or the Na Super Ionic CONductor (NaSICON), to serve as ionic conductors and separators between molten electrodes. Recently, lower-temperature molten Na batteries (100-200 °C) have gained popularity as potential LDES solutions, owing to their promise of high energy and cost-efficiency.[23-40]

Such lower-temperature molten Na batteries face challenging technical requirements before they can be widely adopted for LDES. LDES requires much higher capacity, delivered over longer time periods, and batteries should operate at high power to responsively deliver energy and enable access to a higher active material fraction.[16, 41-44] For LDES batteries using ceramic solid electrolytes, designs are typically limited to planar or tubular geometries, which have relatively

low surface area compared to liquid electrolyte systems, such as Li-ion, that can utilize "jelly-roll" designs. These geometries necessitate much higher current densities (10-100x higher) to achieve high power.[45, 46] For LDES applications, then, low temperature solid electrolytes must accommodate long, continuous discharge at high current densities.

Despite these requirements, many battery studies are performed with limited discharge durations or current densities, resulting in relatively low total discharge capacities. Current densities and discharge durations from recent publications using molten Na metal are compared in **Figure 1**.[24, 28, 31, 34, 35, 37, 38, 47-53]. Values for each point are included in **Table S1**.

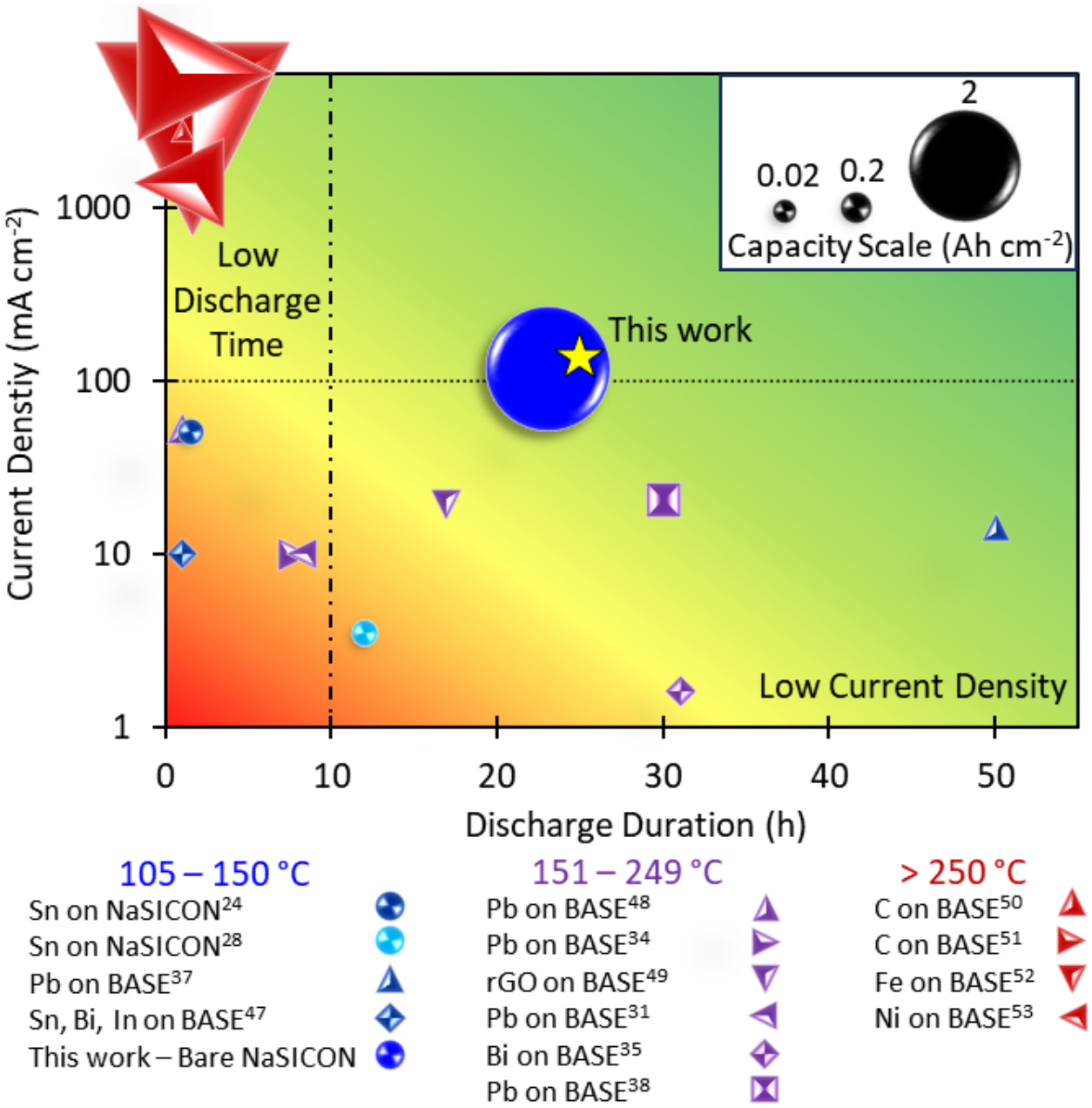

Figure 1. Comparison of the maximum current densities and the maximum discharge durations of previous works. The size of each point represents the maximum half-cycle capacity explored in each work and is not necessarily the product of the maximum current density and the maximum discharge duration (e.g. maximum capacity may have occurred at lower current). The points are color-coded and shaped according to temperature and electrolyte material as noted in the key. Importantly, all previous works used interfacial coatings to mitigate Na metal penetration, whereas this work used uncoated NaSICON under stressful conditions to induce and understand metal penetration mechanisms. Values for each point are included in **Table S1**.

The published data generally fall into two groups: low discharge time or low current density. While currents as high as 5.2 A cm^{-2} have been achieved for short discharge durations (30 min), such high currents must still be demonstrated at long times for validation in LDES. Alternatively, reports applying lower current densities have demonstrated various discharge times, up to 50 h,

though the cycled capacity (indicated by the data point size in **Figure 1**) is still relatively low. This may result from using easily accessible geometries, such as coin cells, that cannot accommodate the capacity necessary for LDES. There has been an expectation that performance in this shorter, low-capacity regime will translate to applications with longer and higher capacity discharges, but this is a risky assumption. Without appropriate LDES testing, important failure mechanisms specific to very high-capacity discharge may not be uncovered.

In this light, we used molten Na symmetric cells (Na|NaSICON|Na) to examine the LDES performance of uncoated NaSICON electrolytes at both high current densities (0.1 A cm^{-2}) *and* long discharge times (up to 23 h), resulting in extremely high capacities (up to 2.3 Ah cm^{-2}). That is, at maximum capacity, a mass of Na 2 cm tall is stripped from one side of the cell and plated onto the other. For practical reasons, uncoated NaSICON was used to create a specific, stressed condition likely to reveal failure behavior under practical test conditions.[24, 54, 55] We particularly focused on assessing degradation or failure as affected by metallic Na penetration through the uncoated NaSICON solid electrolyte. Our results show that long half-cycles lead to significantly accelerated cell failure and that low-capacity galvanostatic cycling cannot capture degradation processes that will likely occur during a single half-cycle in a LDES battery. These findings suggest that half-cycle capacity (Ah cm^{-2}) is a crucial parameter for gauging LDES battery performance.

Symmetric Cell Testing. Na|NaSICON|Na symmetric cells were assembled inside an argon glovebox by filling two glass reservoirs with 4.5 g of Na metal. The cells were placed in a custom oven and uniformly heated to 110 °C for testing. The cell setup can be seen in **Figure S1**. Further symmetric cell and NaSICON synthesis details are available in **Supporting Information**.[24] Symmetric cells were cycled with half-cycle capacities ranging from 0.1 to 2.3 Ah cm^{-2} (hereafter

named NaSICON-x, where x represents half-cycle capacity in Ah cm^{-2}). The 2.3 Ah cm^{-2} half-cycle cell *only transported Na in one direction* throughout the test, though the discharge was broken into 1-hour intervals to allow for electrochemical impedance spectroscopy (EIS) measurements throughout. This unidirectional test enabled observation of impedance changes during a single, extended half-cycle and provided distinct plating and stripping interfaces for dendrite mechanism studies. Shorter half-cycle tests ran essentially the *same total charge* (Ah cm^{-2}) as the long discharge test but alternately reversed the current direction between each shorter half cycle.

After testing, NaSICON pellets were fractured in a bending apparatus (**Figure S2**), designed according to ASTM C1499.[56] Resulting fracture at the pellets' weakest points should have exposed the most significant Na penetration in each pellet.[57] Fractured pellets were transferred to an FEI Quanta 250 field emission scanning electron microscope (SEM) and cross-sections were imaged to investigate the effects of different half-cycle capacities.

The overpotential profiles for NaSICON-0.1, NaSICON-0.4, and NaSICON-2.3 are shown in **Figure 2a**. The overpotential in the NaSICON-0.1 cell was stable during each half-cycle and gradually decreased before reaching a plateau of ~0.4 V near the fifth cycle. The NaSICON-0.4 cell had nearly identical potential plateaus as a function of capacity, just with larger half-cycle capacities. These were in stark contrast to the NaSICON-2.3 cell. After a relatively stable overpotential during the first four unidirectional intervals, the overpotential became increasingly noisy during intervals 5-21. Then, during interval 22, the overpotential sharply decreased to a new plateau, before a steep increase, resulting from disconnection of the stripping Na electrode from the current collector. The overpotential fluctuations were an indication that the extremely high

half-cycle capacity in NaSICON-2.3 leads to degradation *that does not occur* when the cell polarity is frequently reversed at lower half-cycle capacities.

The impedance behaviors of the NaSICON-0.1, NaSICON-04, and NaSICON-2.3 cells are plotted in **Figure 2b**. Specifically, the bulk resistance (R_1) and interfacial resistance (R_2) obtained from EIS fitting are plotted as a function of total capacity (cumulative charge transported in both directions for cycled samples). A few representative Nyquist plots and the equivalent circuit used

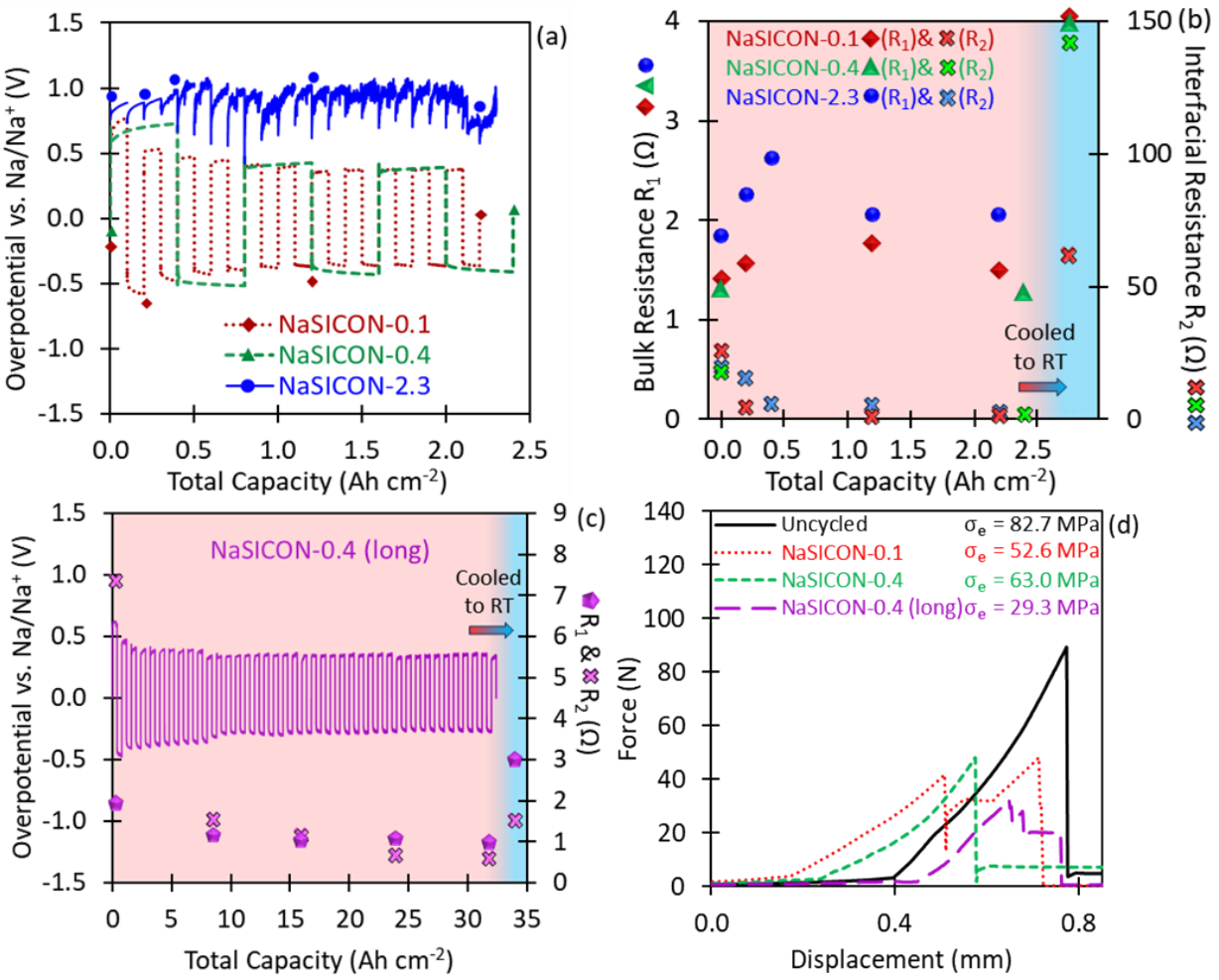

Figure 2. (a) overpotential profiles for NaSICON-0.1, NaSICON-0.4, and NaSICON-2.3 cells tested to 2.3 Ah cm^{-2} total capacity. Markes indicate when EIS measurements shown in (b) were obtained. (b) Bulk (R_1) and interfacial (R_2) resistance values for NaSICON-0.1, NaSICON-0.4, and NaSICON-2.3 cells plotted as a function of capacity. Background color indicates temperature of cell (red = 110 °C, blue = room temp.). (c) Overpotential profile and resistance behavior of NaSICON-0.4(long) cell. Background color indicates temperature (red = 110 °C, blue = room temp). Only resistance measurements (no cycling) were performed at room temperature. (d) Ring-on-ring bending loading profiles and calculated equibiaxial flexural strengths for an uncycled pellet and NaSICON-0.1, NaSICON-0.4, and NaSICON-0.4(long) pellets.

for fitting are shown in **Figure S3**. **Figure 2b** shows that bulk resistance varied little during cycling, maintaining values between 1.3-2.7 Ω throughout testing for all three cells. The interfacial resistance, however, decreased drastically during testing, approaching zero at the end of testing for all three cells. The decreased resistance implied that the Na|NaSICON interfacial contact improved during testing, likely from current application (freshly deposited Na is less resistive) or Na metal penetration into the electrolyte (dendrites).[58-60] Both the NaSICON-0.1 and NaSICON-2.3 cells quickly displayed a reduced interfacial resistance after 0.2 Ah cm^{-2}, likely due to improved wetting.

However, the NaSICON-2.3 cell experienced a second precipitous drop in both bulk and interfacial resistance near 0.4 Ah cm^{-2}, which corresponded with the onset of overpotential fluctuations. We interpreted these fluctuations and coinciding interfacial resistance drop as indicators of significant Na metal penetration in the NaSICON-2.3 cell.

The NaSICON-0.1 cell showed the current-induced reduction in interfacial resistance after 0.2 Ah cm^{-2}, but no further sharp reductions in bulk or interfacial resistance, implying no significant shorting in the cell. This was corroborated by an increased measured impedance for the NaSICON-0.1 cell at room temperature after testing (**Figure 2b**). Cooled to room temperature, the resistance of un-shorted NaSICON increased according to the Arrhenius equation, while the resistance of any Na-shorted NaSICON would have remained low. Similar behavior was observed in the NaSICON-0.4 cell. Since the molten electrode was disconnected from the current collector in the NaSICON-2.3 cell, it was not possible to perform this post-test measurement. Measuring the masses of Na in each reservoir after testing provided further insight into shorting behavior. The NaSICON-0.1 and NaSICON-0.4 cells had the same amount of Na metal in each reservoir at the beginning and end of their tests, implying almost exclusively ionic conduction during testing. In the NaSICON-2.3 cell, only 2.3 g of the theoretical 3.5 g had transferred from the stripping to plating reservoir. Importantly, this suggests that *electronic* conduction through the electrolyte accounted for 34% of the total capacity in the NaSICON-2.3 cell and that it was significantly shorted.

To investigate longer-term cycling behavior, another cell was tested with a half-cycle capacity of 0.4 Ah cm^{-2}, but tested for more cycles, up to 32.4 Ah cm^{-2} total capacity. This cell was named NaSICON-0.4(long) and its overpotential profile is plotted in **Figure 2c**. The overpotential quickly dropped and then maintained a plateau near ~0.4 V, which was nearly identical to the NaSICON-

0.1 and NaSICON-0.4 cells. The impedance response of the NaSICON-0.4(long) cell is also displayed in **Figure 2c** and showed a stable bulk resistance and an interfacial resistance that sharply decreased early in the test. Both resistances increased upon cooling to room temperature (though not as drastically as the NaSICON-0.1 or NaSICON-0.4 cells), implying that electronic conduction through a complete short was not dominating the impedance response. This cell completed testing at an uneven number of half-cycles to determine the fraction of ionic vs. electronic conduction during the final half-cycle and the final Na masses were consistent with predominantly ionic conduction.

To determine the extent of Na penetration, each pellet's cross-section was examined under SEM after being fractured in the bending apparatus. The loading profiles for an uncycled pellet, NaSICON-0.1 pellet, and both NaSICON-0.4 pellets are provided in **Figure 2d**. The fracture load and accompanying fracture strengths in **Figure 2d** show a clear correlation to extent of cycling, with the NaSICON-0.4(long) pellet being the weakest. SEM images and Energy Dispersive X-Ray Spectroscopy (EDS) maps of selected regions are shown in **Figure 3**. In the NaSICON-0.1 pellet (**Figure 3a**), small dark regions were observed dispersed throughout the cross-section. These contrasted the bright, cube-like grains of NaSICON observed in most of the cross-section. A pristine cross-section is shown for comparison in **Figure S4**. Previous studies have identified these dark regions as Na-rich and indicators of Na penetration.[54] EDS, however, did not show the regions in the NaSICON-0.1 pellet as Na-rich, despite microstructural similarity to previously identified Na spots. We hypothesize that upon reversing the polarity of the cell at 0.1 Ah cm^{-2}, Na penetration during the first half-cycle *could be partially stripped away* on the reverse cycle. This leads to minimal net accumulation of Na in the electrolyte. This process could repeat during subsequent half-cycles, minimizing *permanent* Na penetration during cycling.

Interestingly, many of these dark regions appeared isolated from either interface, implying one of two things: (1) ion-electron recombination (classically, Mode II degradation) led to the formation of Na "islands" in the electrolyte or (2) reversal of Na penetration at the plating interface (classically, Mode I degradation) led to the isolation of these Na islands.[61] Mode II degradation has recently been proposed as a significant degradation mode in solid electrolytes and dendrite

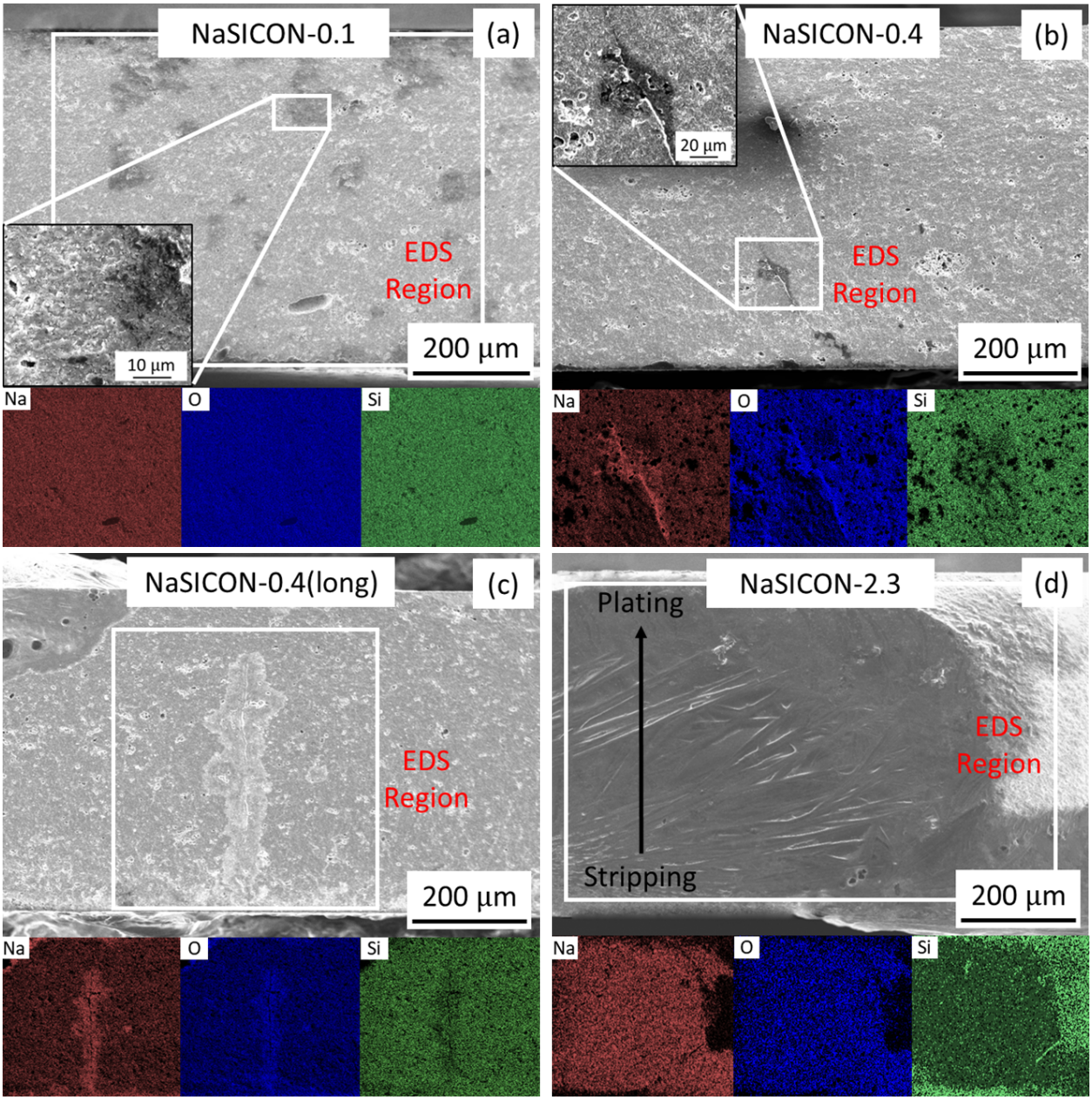

Figure 3. SEM images and EDS maps of (a) NaSICON-0.1 (b) NaSICON-0.4 (to 2.4 Ah cm^{-2}) (c) NaSICON-0.4 (to 32.4 Ah cm^{-2}) and (d) NaSICON-2.3. For (a) & (d) the entire image is included in the EDS mapping.

disconnection from metal anodes (to form "dead" Li) has been observed in Li-ion cells, so both mechanisms likely contributed to the island formation.[54, 58, 59]

The NaSICON-0.4 cells displayed slightly different behavior. Instead of the small, disconnected dark regions seen in the NaSICON-0.1 cell, the NaSICON-0.4 cells (**Figure 3b-c)** contained a few dendritic features extended more significantly into the cross-section. These were clearly identified as Na metal penetration *via* EDS. These longer dendritic features suggested a transition to primarily Mode I degradation. The larger half-cycle capacity and fewer polarity reversals allowed these dendrites to grow longer without recovery. This is most obvious in the NaSICON-0.4(long) pellet, which showed individual dendrites that nearly traversed the electrolyte, explaining the relatively lower resistance upon cooling in **Figure 2c** and low bending strength in **Figure 2d**. This transition between failure mechanisms highlights the importance of half-cycle capacity when testing LDES batteries.

The NaSICON-2.3 pellet (**Figure 3d**) exhibited dramatic Na penetration. A large region of the pellet was filled with Na metal and clearly correlated with the fluctuating potential and resistance drops observed in **Figure 2b**. It was difficult to ascertain the initiation point of the Na metal here due to connection between interfaces and it could be reasonably concluded that both Mode I and Mode II contributed to the Na penetration, based on previous observations.[54] This further exemplifies the shortcomings of traditional, low-capacity cycling tests, which do not capture the prevalent failure mechanisms that can occur during LDES applications.

The proposed behaviors in low and high half-cycle capacity tests are illustrated in **Scheme 1**. All cells quickly experience some degree of Na penetration upon applying current through uncoated NaSICON, either from Mode I or II penetration. In low half-cycle capacity cells, this penetration can be partially "healed" upon reversing polarity during cycling, leading to minimal permanent Na penetration. A related "healing" phenomenon has been observed in liquid electrolyte Li-ion batteries, where researchers observed that dendrites can be reversibly stripped away during galvanostatic cycling when cell polarity is reversed.[58, 59] However, in cells tested at higher half-cycle capacities, Na metal that penetrates the electrolyte has sufficient time to grow and extend through the cross-section, eventually leading to failure. The healing process at lower half-cycle capacities can therefore artificially inflate the observed cycling life during testing and misrepresent the true LDES capability of a solid electrolyte. This theoretical image stresses the importance of tailoring LDES testing procedures to fit their intended application.

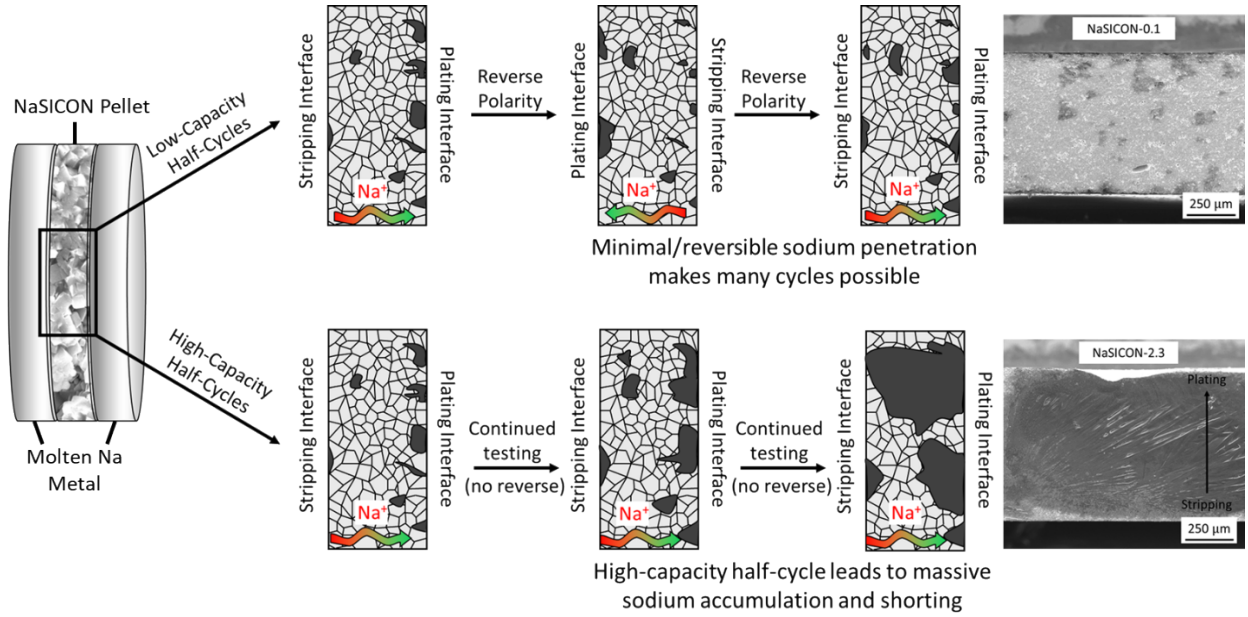

Scheme 1. Illustration of proposed behavior in cells cycled with low- and high-capacity half-cycles. Darker spots in the cartoon represent Na metal penetration.

New battery materials and chemistries will continue to be developed and tested in candidate LDES technologies. Traditional low-capacity testing, however, may not accurately assess true material

viability due to the massive increase in half-cycle capacity necessary for LDES. Herein, we demonstrated that high half-cycle capacities (long-discharge times) lead to fundamentally different failure mechanisms in uncoated NaSICON, even when tested at the same current density *and* total capacity as shorter-duration tests. Our results showed that cycling cells at lower half-cycle capacities (0.1-0.4 Ah cm^{-2}) resulted in minimal Na penetration and a long cycle life (> 32.4 Ah cm^{-2} total). However, at extremely high half-cycle capacities (up to 2.3 Ah cm^{-2}), the NaSICON pellet was shorted during a single half-cycle. These findings underline the importance of examining a critical (dis)charge capacity (Ah cm^{-2}), in addition to the well-studied critical current density (A cm^{-2}). Including this consideration in routine testing for LDES batteries will ensure that testing at lab-scale accurately simulates the harsh conditions they will undergo in deployment.

ASSOCIATED CONTENT

Accompanying numerical data for **Figure 1**, symmetric cell schematic and detailed setup information, detailed NaSICON synthesis procedure, detailed ring-on-ring bending schematic and procedure, representative Nyquist plots from tested cells, and image of a pristine NaSICON cross-section after fracture during ring-on-ring bending. (PDF)

AUTHOR INFORMATION

Ryan Hill

Department of Chemical and Materials Engineering

University of Kentucky College of Engineering

177 F Paul Anderson Tower

512 Administration Drive

Lexington, KY 40506

Ryan.C.Hill@uky.edu

Notes

Present Addresses

†Ryan Hill is now at Stony Brook University (Stony Brook, NY, USA).

ACKNOWLEDGMENT

This work was conducted through a collaboration between the University of Kentucky and Sandia National Laboratories and was supported by the Energy Storage Program, managed by Dr. Imre Gyuk, in the U.S. Department of Energy's Office of Electricity. Sandia National Laboratories is a multi-mission laboratory managed and operated by National Technology & Engineering Solutions of Sandia, LLC (NTESS), a wholly owned subsidiary of Honeywell International Inc., for the U.S. Department of Energy's National Nuclear Security Administration (DOE/NNSA) under contract DE-NA0003525. This written work is authored by an employee of NTESS. The employee, not NTESS, owns the right, title and interest in and to the written work and is responsible for its contents. Any subjective views or opinions that might be expressed in the written work do not necessarily represent the views of the U.S. Government. The publisher acknowledges that the U.S. Government retains a non-exclusive, paid-up, irrevocable, world-wide license to publish or reproduce the published form of this written work or allow others to do so, for U.S. Government

purposes. The DOE will provide public access to results of federally sponsored research in accordance with the DOE Public Access Plan.

REFERENCES

(1) Casper, J. K. *Fossil fuels and pollution: the future of air quality*; Infobase Publishing, 2010.

(2) Liu, L.; Cheng, S. Y.; Li, J. B.; Huang, Y. F. Mitigating Environmental Pollution and Impacts from Fossil Fuels: The Role of Alternative Fuels. *Energy Sources, Part A: Recovery, Utilization, and Environmental Effects* **2007**, *29* (12), 1069-1080. DOI: 10.1080/15567030601003627.

(3) Odeh, N. A.; Cockerill, T. T. Life cycle GHG assessment of fossil fuel power plants with carbon capture and storage. *Energy Policy* **2008**, *36* (1), 367-380. DOI: https://doi.org/10.1016/j.enpol.2007.09.026.

(4) Ediger, V. Ş. An integrated review and analysis of multi-energy transition from fossil fuels to renewables. *Energy Procedia* **2019**, *156*, 2-6. DOI: https://doi.org/10.1016/j.egypro.2018.11.073.

(5) Ackermann, T.; Söder, L. Wind energy technology and current status: a review. *Renewable and Sustainable Energy Reviews* **2000**, *4* (4), 315-374. DOI: https://doi.org/10.1016/S1364-0321(00)00004-6.

(6) Anvari, M.; Lohmann, G.; Wächter, M.; Milan, P.; Lorenz, E.; Heinemann, D.; Tabar, M. R. R.; Peinke, J. Short term fluctuations of wind and solar power systems. *New Journal of Physics* **2016**, *18* (6), 063027. DOI: 10.1088/1367-2630/18/6/063027.

(7) Calero, I.; Cañizares, C. A.; Bhattacharya, K.; Baldick, R. Duck-Curve Mitigation in Power Grids With High Penetration of PV Generation. *IEEE Transactions on Smart Grid* **2022**, *13* (1), 314-329. DOI: 10.1109/TSG.2021.3122398.

(8) Kosowatz, J. Energy Storage Smooths the Duck Curve. *Mechanical Engineering* **2018**, *140* (06), 30-35. DOI: 10.1115/1.2018-JUN-1 (acccessed 8/20/2023).

(9) Moran, E. F.; Lopez, M. C.; Moore, N.; Müller, N.; Hyndman, D. W. Sustainable hydropower in the 21st century. *Proceedings of the National Academy of Sciences* **2018**, *115* (47), 11891-11898. DOI: 10.1073/pnas.1809426115.

(10) Rahman, M. M.; Oni, A. O.; Gemechu, E.; Kumar, A. Assessment of energy storage technologies: A review. *Energy Convers. Manage.* **2020**, *223*, 113295. DOI: https://doi.org/10.1016/j.enconman.2020.113295.

(11) Denholm, P.; Nunemaker, J.; Gagnon, P.; Cole, W. The potential for battery energy storage to provide peaking capacity in the United States. *Renewable Energy* **2020**, *151*, 1269-1277. DOI: https://doi.org/10.1016/j.renene.2019.11.117.

(12) *The Journey to Net-zero: An Action Plan to Unlock a Secure, Net-zero Power System*; Long Duration Energy Storage Council, 2022.

(13) *World Energy Outlook 2022*; International Energy Agency, Paris, 2022.

(14) Denholm, P.; Cole, W.; Blair, N. Moving Beyond 4-Hour Li-Ion Batteries: Challenges and Opportunities for Long (er)-Duration Energy Storage. **2023**.

(15) Guerra, O. J. Beyond short-duration energy storage. *Nat. Energy* **2021**, *6* (5), 460-461.

(16) Albertus, P.; Manser, J. S.; Litzelman, S. Long-Duration Electricity Storage Applications, Economics, and Technologies. *Joule* **2020**, *4* (1), 21-32. DOI: https://doi.org/10.1016/j.joule.2019.11.009.

(17) Kebede, A. A.; Coosemans, T.; Messagie, M.; Jemal, T.; Behabtu, H. A.; Van Mierlo, J.; Berecibar, M. Techno-economic analysis of lithium-ion and lead-acid batteries in stationary energy storage application. *Journal of Energy Storage* **2021**, *40*, 102748. DOI: https://doi.org/10.1016/j.est.2021.102748.

(18) Helbig, C.; Bradshaw, A. M.; Wietschel, L.; Thorenz, A.; Tuma, A. Supply risks associated with lithium-ion battery materials. In *Journal of Cleaner Production*, Elsevier Ltd: 2018; Vol. 172, pp 274-286.

(19) Wentker, M.; Greenwood, M.; Asaba, M. C.; Leker, J. A raw material criticality and environmental impact assessment of state-of-the-art and post-lithium-ion cathode technologies. In *Journal of Energy Storage*, Elsevier Ltd: 2019; Vol. 26, p 101022.

(20) Chen, Y.; Kang, Y.; Zhao, Y.; Wang, L.; Liu, J.; Li, Y.; Liang, Z.; He, X.; Li, X.; Tavajohi, N.; Li, B. A review of lithium-ion battery safety concerns: The issues, strategies, and testing standards. *Journal of Energy Chemistry* **2021**, *59*, 83-99. DOI: https://doi.org/10.1016/j.jechem.2020.10.017.

(21) Kummer, J. T.; Weber, N. A sodium-sulfur secondary battery. *Sae Transactions* **1968**, 1003-1028.

(22) Coetzer, J. A new high energy density battery system. *J. Power Sources* **1986**, *18* (4), 377-380. DOI: https://doi.org/10.1016/0378-7753(86)80093-3.

(23) Small, L. J.; Eccleston, A.; Lamb, J.; Read, A. C.; Robins, M.; Meaders, T.; Ingersoll, D.; Clem, P. G.; Bhavaraju, S.; Spoerke, E. D. Next generation molten NaI batteries for grid scale energy storage. *J. Power Sources* **2017**, *360*, 569-574. DOI: https://doi.org/10.1016/j.jpowsour.2017.06.038.

(24) Gross, M. M.; Small, L. J.; Peretti, A. S.; Percival, S. J.; Rodriguez, M. A.; Spoerke, E. D. Tin-based ionic chaperone phases to improve low temperature molten sodium-NaSICON interfaces. *J. Mater. Chem. A* **2020**, *8*, 17012-17018. DOI: 10.1039/d0ta03571h.

(25) Gross, M. M.; Percival, S. J.; Small, L. J.; Lamb, J.; Peretti, A. S.; Spoerke, E. D. Low-Temperature Molten Sodium Batteries. *ACS Applied Energy Materials* **2020**, *3* (11), 11456-11462. DOI: 10.1021/acsaem.0c02385.

(26) Gross, M. M.; Percival, S. J.; Lee, R. Y.; Peretti, A. S.; Spoerke, E. D.; Small, L. J. A high-voltage, low-temperature molten sodium battery enabled by metal halide catholyte chemistry. *Cell Rep Phys Sci* **2021**, *2* (7). DOI: ARTN 100489 10.1016/j.xcrp.2021.100489.

(27) Spoerke, E. D.; Gross, M. M.; Percival, S. J.; Small, L. J. Molten Sodium Batteries. In *Energy-Sustainable Advanced Materials*, Alston, M., Lambert, T. N. Eds.; Springer International Publishing, 2021; pp 59-84.

(28) Maraschky, A. M.; Meyerson, M. L.; Percival, S. J.; Lowry, D. R.; Meserole, S.; Williard, J. N.; Peretti, A. S.; Gross, M.; Small, L. J.; Spoerke, E. D. Impact of Catholyte Lewis Acidity at the Molten Salt–NaSICON Interface in Low-Temperature Molten Sodium Batteries. *The Journal of Physical Chemistry C* **2023**, *127* (3), 1293-1302. DOI: 10.1021/acs.jpcc.2c06240.

(29) Maraschky, A. M.; Percival, S. J.; Lee, R. Y.; Meyerson, M. L.; Peretti, A. S.; Spoerke, E. D.; Small, L. J. Electrode Blocking Due to Redox Reactions in Aluminum Chloride-Sodium Iodide Molten Salts. *J. Electrochem. Soc.* **2023**, *170* (6), 066504. DOI: 10.1149/1945-7111/acd874.

(30) Lu, X.; Li, G.; Kim, J. Y.; Lemmon, J. P.; Sprenkle, V. L.; Yang, Z. The effects of temperature on the electrochemical performance of sodium–nickel chloride batteries. *J. Power Sources* **2012**, *215*, 288-295. DOI: https://doi.org/10.1016/j.jpowsour.2012.05.020.

(31) Lu, X.; Li, G.; Kim, J. Y.; Mei, D.; Lemmon, J. P.; Sprenkle, V. L.; Liu, J. Liquid-metal electrode to enable ultra-low temperature sodium–beta alumina batteries for renewable energy storage. *Nat. Commun.* **2014**, *5* (1). DOI: 10.1038/ncomms5578.

(32) Li, G.; Lu, X.; Kim, J. Y.; Viswanathan, V. V.; Meinhardt, K. D.; Engelhard, M. H.; Sprenkle, V. L. An Advanced Na–$FeCl_2$ ZEBRA Battery for Stationary Energy Storage Application. *Adv. Energy Mater.* **2015**, *5* (12), 1500357. DOI: https://doi.org/10.1002/aenm.201500357.

(33) Li, G.; Lu, X.; Kim, J. Y.; Meinhardt, K. D.; Chang, H. J.; Canfield, N. L.; Sprenkle, V. L. Advanced intermediate temperature sodium–nickel chloride batteries with ultra-high energy density. *Nat. Commun.* **2016**, *7* (1), 10683. DOI: 10.1038/ncomms10683.

(34) Chang, H. J.; Lu, X.; Bonnett, J. F.; Canfield, N. L.; Han, K.; Engelhard, M. H.; Jung, K.; Sprenkle, V. L.; Li, G. Decorating β″-alumina solid-state electrolytes with micron Pb spherical particles for improving Na wettability at lower temperatures. *J. Mater. Chem. A* **2018**, *6*, 19703-19711. DOI: 10.1039/C8TA06745G.

(35) Jin, D.; Choi, S.; Jang, W.; Soon, A.; Kim, J.; Moon, H.; Lee, W.; Lee, Y.; Son, S.; Park, Y.-C.; et al. Bismuth Islands for Low-Temperature Sodium-Beta Alumina Batteries. *ACS Appl. Mater. Interfaces* **2019**, *11* (3), 2917-2924. DOI: 10.1021/acsami.8b13954.

(36) Zhan, X.; Bowden, M. E.; Lu, X.; Bonnett, J. F.; Lemmon, T.; Reed, D. M.; Sprenkle, V. L.; Li, G. A Low-Cost Durable Na-$FeCl_2$ Battery with Ultrahigh Rate Capability. *Adv. Energy Mater.* **2020**, *10* (10), 1903472. DOI: https://doi.org/10.1002/aenm.201903472.

(37) Li, M. M.; Tripathi, S.; Polikarpov, E.; Canfield, N. L.; Han, K. S.; Weller, J. M.; Buck, E. C.; Engelhard, M. H.; Reed, D. M.; Sprenkle, V. L.; Li, G. Interfacial Engineering with a Nanoparticle-Decorated Porous Carbon Structure on β″-Alumina Solid-State Electrolytes for Molten Sodium Batteries. *ACS Appl. Mater. Interfaces* **2022**, *14* (22), 25534-25544. DOI: 10.1021/acsami.2c05245.

(38) Weller, J. M.; Li, M. M.; Polikarpov, E.; Han, K. S.; Kidner, N.; Patel, A.; Nguyen, M.; Stout, M.; Gossett, M.; Jung, K.; et al. Unlocking the NaCl-$AlCl_3$ phase diagram for low-cost, long-duration Na-Al batteries. *Energy Storage Materials* **2023**, *56*, 108-120. DOI: https://doi.org/10.1016/j.ensm.2023.01.009.

(39) Kim, J.; Jo, S. H.; Bhavaraju, S.; Eccleston, A.; Kang, S. O. Low temperature performance of sodium–nickel chloride batteries with NaSICON solid electrolyte. *J. Electroanal. Chem.* **2015**, *759*, 201-206. DOI: https://doi.org/10.1016/j.jelechem.2015.11.022.

(40) Flynn, A.; Taggert, D.; Johnston, J.; Christensen, M.; Makowski, M.; Moss, R.; Kathiria, R.; Bhavaraju, S.; Hughes, S. Novel Sodium – Polysulfide Flow Battery Grid-scale Energy Storage Technology. In *2022 IEEE Electrical Energy Storage Application and Technologies Conference (EESAT)*, 8-9 Nov. 2022, 2022; pp 1-3. DOI: 10.1109/EESAT55007.2022.9998026.

(41) Akhil, A. A.; Huff, G.; Currier, A. B.; Kaun, B. C.; Rastler, D. M.; Chen, S. B.; Cotter, A. L.; Bradshaw, D. T.; Gauntlett, W. D. *DOE/EPRI 2013 electricity storage handbook in collaboration with NRECA*; Sandia National Laboratories Albuquerque, NM, USA, 2013.

(42) Denholm, P.; Hand, M. Grid flexibility and storage required to achieve very high penetration of variable renewable electricity. *Energy Policy* **2011**, *39* (3), 1817-1830. DOI: https://doi.org/10.1016/j.enpol.2011.01.019.

(43) Denholm, P.; Mai, T. Timescales of energy storage needed for reducing renewable energy curtailment. *Renewable Energy* **2019**, *130*, 388-399. DOI: https://doi.org/10.1016/j.renene.2018.06.079.

(44) Ziegler, M. S.; Mueller, J. M.; Pereira, G. D.; Song, J.; Ferrara, M.; Chiang, Y.-M.; Trancik, J. E. Storage Requirements and Costs of Shaping Renewable Energy Toward Grid Decarbonization. *Joule* **2019**, *3* (9), 2134-2153. DOI: https://doi.org/10.1016/j.joule.2019.06.012.

(45) Lu, X.; Li, G.; Meinhardt, K. D.; Sprenkle, V. L. *Development of Na-beta alumina batteries at Pacific Northwest National Laboratory: From tubular to planar*; Pacific Northwest National Lab.(PNNL), Richland, WA (United States), 2016.

(46) Lan, T.; Graeber, G.; Sieuw, L.; Svaluto-Ferro, E.; Vagliani, F.; Basso, D.; Turconi, A.; Battaglia, C.; Heinz, M. V. F. Planar Sodium-Nickel Chloride Batteries with High Areal Capacity for Sustainable Energy Storage. *Adv. Funct. Mater.* **2023**, *33* (33), 2302040. DOI: https://doi.org/10.1002/adfm.202302040.

(47) Ahlbrecht, K.; Bucharsky, C.; Holzapfel, M.; Tübke, J.; Hoffmann, M. J. Investigation of the wetting behavior of Na and Na alloys on uncoated and coated Na-β”-alumina at temperatures below 150 °C. *Ionics* **2017**, *23* (5), 1319-1327. DOI: 10.1007/s11581-017-2017-x.

(48) Jung, K.; Chang, H.-J.; Bonnett, J. F.; Canfield, N. L.; Sprenkle, V. L.; Li, G. An advanced Na-$NiCl_2$ battery using bi-layer (dense/micro-porous) β″-alumina solid-state electrolytes. *J. Power Sources* **2018**, *396*, 297-303. DOI: https://doi.org/10.1016/j.jpowsour.2018.06.039.

(49) Jin, D.; Lee, H. G.; Choi, S.; Kim, S.; Lee, Y.; Son, S.; Park, Y.-C.; Lee, J. S.; Jung, K.; Shim, W. Sparked Reduced Graphene Oxide for Low-Temperature Sodium-Beta Alumina Batteries. *Nano Lett.* **2019**, *19* (12), 8811-8820. DOI: 10.1021/acs.nanolett.9b03646.

(50) Landmann, D.; Graeber, G.; Heinz, M. V. F.; Haussener, S.; Battaglia, C. Sodium plating and stripping from Na-β"-alumina ceramics beyond 1000 mA/cm^2. *Mater. Today Energy* **2020**, *18*, 100515. DOI: 10.1016/J.MTENER.2020.100515.

(51) Hu, Y.; Wen, Z.; Wu, X.; Jin, J. Low-cost shape-control synthesis of porous carbon film on β″-alumina ceramics for Na-based battery application. *J. Power Sources* **2012**, *219*, 1-8. DOI: https://doi.org/10.1016/j.jpowsour.2012.07.025.

(52) Hu, Y.; Wen, Z.; Wu, X. Porous iron oxide coating on β″-alumina ceramics for Na-based batteries. *Solid State Ionics* **2014**, *262*, 133-137. DOI: https://doi.org/10.1016/j.ssi.2013.08.033.

(53) Hu, Y.; Wen, Z.; Wu, X.; Lu, Y. Nickel nanowire network coating to alleviate interfacial polarization for Na-beta battery applications. *J. Power Sources* **2013**, *240*, 786-795. DOI: https://doi.org/10.1016/j.jpowsour.2013.04.056.

(54) Hill, R.; Peretti, A.; Small, L. J.; Spoerke, E. D.; Cheng, Y.-T. Molten Sodium Penetration in NaSICON Electrolytes at 0.1 A cm^{-2}. *ACS Applied Energy Materials* **2023**, *6* (4), 2515-2523. DOI: 10.1021/acsaem.2c03944.

(55) Hill, R.; Peretti, A.; Maraschky, A. M.; Small, L. J.; Spoerke, E. D.; Cheng, Y.-T. Can a Coating Mitigate Molten Na Dendrite Growth in NaSICON Under High Current Density. *In Review* **2023**.

(56) ASTM International. *Standard Test Method for Monotonic Equibiaxial Flexural Strength of Advanced Ceramics at Ambient Temperature*; West Conshohocken, PA, 2019.

(57) She, S.; Landes, J. D.; Boulet, J. A. M.; Stoneking, J. E. Statistical Theory for Predicting the Failure of Brittle Materials. *Journal of Applied Mechanics* **1991**, *58* (1), 43-49. DOI: 10.1115/1.2897177 (acccessed 8/22/2023).

(58) Wood, K. N.; Kazyak, E.; Chadwick, A. F.; Chen, K.-H.; Zhang, J.-G.; Thornton, K.; Dasgupta, N. P. Dendrites and Pits: Untangling the Complex Behavior of Lithium Metal Anodes through Operando Video Microscopy. *ACS Cent. Sci.* **2016**.

(59) Chen, K. H.; Wood, K. N.; Kazyak, E.; Lepage, W. S.; Davis, A. L.; Sanchez, A. J.; Dasgupta, N. P. Dead lithium: Mass transport effects on voltage, capacity, and failure of lithium metal anodes. *J. Mater. Chem. A* **2017**, *5*, 11671-11681. DOI: 10.1039/C7TA00371D.

(60) Kazyak, E.; Garcia-Mendez, R.; LePage, W. S.; Sharafi, A.; Davis, A. L.; Sanchez, A. J.; Chen, K. H.; Haslam, C.; Sakamoto, J.; Dasgupta, N. P. Li Penetration in Ceramic Solid Electrolytes: Operando Microscopy Analysis of Morphology, Propagation, and Reversibility. *Matter* **2020**, *2*, 1025-1048. DOI: 10.1016/J.MATT.2020.02.008.

(61) De Jonghe, L. C.; Feldman, L.; Buechele, A. Failure modes of Na-beta alumina. *Solid State Ionics* **1981**, *5*, 267-269. DOI: 10.1016/0167-2738(81)90244-7.